atoms

MDPI

Communication

Differential Description of Multiple Ionization of Uracil by 3.5 MeV/u C^{6+} Impact

N. D. Cariatore *, N. Bachi and S. Otranto

Instituto de Física del Sur (IFISUR), Departamento de Física, Universidad Nacional del Sur (UNS), CONICET, Av. L. N. Alem 1253, Bahía Blanca B8000, Argentina
* Correspondence: nelson.cariatore@uns.edu.ar

Abstract: In this work, a theoretical analysis of the impact of the multiple ionization of uracil by 3.5 MeV/u C^{6+} is developed in the framework of a classical trajectory Monte Carlo method, as recently introduced for multi-electronic targets. The electron emission contribution arising from the multiple electron ionization is explicitly determined and the emission geometries and the reaction regions for double and triple ionization are explicitly identified. The present results suggest that double ionization is mainly characterized by the emission of slow electrons with a relative angle of 80°–120°. For triple ionization, on the other hand, the emission seems to occur with the three electrons holding similar interelectronic angles.

Keywords: multiple ionization; uracil; ion-molecule collisions; classical trajectory Monte Carlo

1. Introduction

The role played by collision processes between highly charged ions and molecules in fields such as astrophysics, fusion plasma and radiotherapy, among others, have stimulated their ample study for decades. In astrophysics, charge exchange has been found to play a preponderant role in the x-ray emission from comets and planetary environments. In these contexts, the photonic emission results from the de-excitation of the solar wind ions which have captured electrons from gas phase targets such as H_2O, CO, and CO_2 among others [1–3]. Another field where this process plays a relevant role is fusion plasmas. Here, line emission cross-sections in the visible range, which contain information on the photonic emissions that follow charge exchange reactions, are used for plasma diagnostics inside tokamaks [4]. Relevant parameters such as the temperature, the presence of impurities and the level of rotation experienced by the plasma are therefore inferred from these data.

Ionization, on the other hand, is known to be particularly relevant in radiotherapy. Either based on photon, electron, or ion impact, radiotherapy pursues the objective of killing tumor cells via single and multiple ionization processes. In fact, it is currently accepted that multiple strand breaks in DNA ultimately lead to tumor cell death. However, the mediating physical mechanisms in such a multi-scale process, in temporal terms, are not yet known and deserve attention from the basic physics perspective. Despite the fact that the ion-therapy technique was proposed by Robert Wilson back in 1946, the experimental measurements of cross-sections for ion collisions with biological targets are still limited. While for most purposes H_2O has been used as a potential substitute for biological tissue and has been intensively studied [3,5–16], RNA bases, on the other hand, have become objects of study in recent years. It is worth noting that, from the experimental point of view, only uracil has been analyzed at the total, single differential, and double differential level at present [16–25]. In principle, single differential cross-sections in energy provide sufficient information to calculate the stopping power; however, the projectile linear energy transfer, the Bragg peak, and the Monte Carlo track structure codes that mimic the irradiation process make use of doubly differential cross-sections to characterize the electron emissions that

check for updates

Citation: Cariatore, N.D.; Bachi, N.; Otranto, S. Differential Description of Multiple Ionization of Uracil by 3.5 MeV/u C^{6+} Impact. *Atoms* **2023**, *11*, 38. https://doi.org/10.3390/atoms11020038

Academic Editor: Károly Tőkési

Received: 9 January 2023
Revised: 2 February 2023
Accepted: 9 February 2023
Published: 11 February 2023

take place along the projectile path. By doing so, in principle, a more accurate description of the radial dose distribution is achieved [8].

From the theoretical side, distorted wave methods such as the first Born approximation with correct boundary conditions (CB1), the continuum-distorted-wave eikonal initial state (CDW-EIS) [21], the *n*-electron classical trajectory Monte Carlo method (nCTMC) [26], the classical over-barrier classical trajectory Monte Carlo (COB-CTMC) [25], the multicenter CTMC approach [20], the independent atom model-pixel counting method (IAM-PCM) [16,24], and the classical trajectory Monte Carlo (CTMC) method in a one-active electron treatment married to binomial statistical rules [14,15] have been largely employed to treat H_2O and RNA bases alike.

In a recent work, we presented an adaptive CTMC model (Ad-CTMC) to treat the multiple ionization of gas-phase H_2O by the impact of highly charged ions [13]. There, eight electrons were explicitly considered and assumed to evolve in the mean field created by the nuclei and the other electrons. The interelectronic correlations were not considered in our treatment to avoid the well-known classical instability of atomic/molecular targets.

Whenever an electron was removed, the remaining target ion was dynamically adapted by assuming vertical energetic transitions. This procedure guarantees the proper energy transfer to the target for multiple electron removal. Simultaneously, the correct number of electrons per orbital was considered at all times. This model has been recently extended for uracil targets, leading to good agreement with the reported experimental data for ionization following 3.5 MeV/u C^{6+} impact, at the total, singly differential and doubly differential levels [27].

In this work, we further extend our analysis on the 3.5 MeV/u C^{6+} + uracil collision system, and analyze the double- and triple-ionization emission geometries and the corresponding extension of the reaction region for these processes. In Section 2, the theoretical method employed in this work was briefly described. The results are shown and discussed in Section 3. Finally, conclusions are drawn in Section 4. Atomic units are used throughout this work unless otherwise stated.

2. Theoretical Method

Ad-CTMC Method

For each molecular orbital of uracil, and for each trajectory, we initialize the system by sorting an electron between the different molecular centers based on Mulliken's populations. The electrons are initialized using microcanonical distributions [28–30]. In our treatment, each electron interacts in the first stage of the simulation with only one center j of the molecular orbital, to which it is bound via the potential developed by Garvey et al. [31] based on Hartree–Fock calculations:

$$V_{Gq}(r_{ij}) = -\frac{Z_j - (N_j - 1)\left(1 - \Omega_j(r_{ij})\right)}{r_{ij}} \quad (1)$$

$$\Omega_j(r_{ij}) = \left[\left(\frac{\eta_j}{\xi_j}\right)(e^{\xi_j r_{ij}} - 1) + 1\right]^{-1}, \quad (2)$$

where the variable r_{ij} represents the distance between the electron i and the center j, Z_j is the nuclear charge of the molecular orbital center j, and $N_j - 1$ is the corresponding number of screening electrons. The parameters ξ_j and η_j are those tabulated by Garvey et al. for the atom conforming the j-center (C, N, O, or H). The subindex q denotes the asymptotic charge of center j experienced by the electron i.

The electronic orbitals of uracil are statistically generated as the number of sorted trajectories becomes large. In ref. [27], we showed that the electronic densities are found to be in good agreement with the quantal description, aside from the lack of nodal structures in the classical description where more circular-shaped structures are observed.

Due to computational limitations, we restricted our analysis to one electron per orbital, thus leading to the numerical solution of Hamilton equations for a system considering

21 electrons. Since the present experimental setups used to determine cross-sections at the total, single differential, and doubly differential levels cannot resolve over the molecular orientations, we randomly orientated the uracil molecule via an Euler rotation. The present treatment allows for a differential analysis of multiple ionization events, in contrast to the one-active electron treatments used for H_2O and uracil targets to date [6,14,15,23].

The lack of description of the interelectronic interactions throughout the simulation, despite providing stability to the multi-electronic target, leads to a considerable number of multiple ionization events associated with the energy transfers which are lower than those provided by the vertical transitions among the different molecular ionic states. In order to correct this issue, we implement a resorting procedure following each electronic emission that we now describe. Whenever an electron acquires a positive value for its energy relative to the target, the electron is assumed to have been emitted and its interactions with the bound electrons and the remaining nuclei of the molecular orbital are explicitly turned on. In this situation, the emitted electron interacts with the remaining nuclei via the potentials V_{Gq} whose parameterizations correspond to $q = 0$. Simultaneously, the remaining target electrons are re-sorted anew assuming vertical energetic transitions to the new molecular orbitals for the molecular ion. These new molecular orbitals are calculated via the GAMESS software [32]. Again, electrons are sorted in the molecular orbitals for the uracil^{+q} ion according to their Mulliken populations. The whole process is then repeated whenever electrons are removed from the target. By doing so, the molecular contraction dynamics that follows each electron removal event is explicitly considered in the collisional dynamics. Moreover, as soon as an electron is identified as "emitted", its postcollisional interaction with those previously emitted is turned on. Molecular orbitals for uracil ions with an odd charge state were calculated by means of the Restricted–Open Shell–Hartree–Fock method (ROHF), and those with and even charge state by the RHF method.

The net singly differential cross-sections (SDCS) in energy and angle are calculated as follows:

$$\begin{aligned} \frac{d\sigma_{net}}{d\varepsilon} &= \frac{N_{ion}(E_i)}{N_{tot}} \frac{1}{\Delta E_i} \pi\, b_{max}^2, \\ \frac{d\sigma_{net}}{d\Omega} &= \frac{N_{ion}(\theta_i)}{N_{tot}} \frac{1}{\Delta \Omega} \pi\, b_{max}^2, \end{aligned} \tag{3}$$

where N_{tot} is the total number of trajectories run within a given maximum impact parameter b_{max}, N_{ion} is the number of positive ionization events, and Ω is the solid angle where the electronic emission is measured.

Since the asymptotic momenta of all the emitted electrons are explicitly analyzed for each ionization event, the separation of the single and the different multiple ionization contributions in Equation (3) is straightforward.

3. Results and Discussion

In Figure 1, we show the SDCS as a function of the angle and the energy of the emitted electron. The results obtained with the present Ad-CTMC model are compared with the experimental data of Agnihotri et al. [21]. Separate contributions from the single-, double-, triple-, and higher-order ionizations are explicitly shown. It can be seen that while in angular terms the contributions from the different mechanisms are similar in shape, the SDCS in energy clearly reveals that single ionization dominates the low emission energy region, while the joint contributions from multiple ionization channels turn dominant as the electron emission energy is greater than approximately 25 eV. We also included the Auger KLL peak contributions to the net SDCS provided by the Ad-CTMC. For this purpose, we assumed an isotropic distribution for these peaks and estimated their intensities from the total ionization cross-sections for the K-shell electrons of C, N, and O obtained using a three-body CTMC code. The resulting intensities were convoluted by means of Gaussian functions centered around the respective KLL Auger peak energies with a full width at half-maximum of 30 eV.

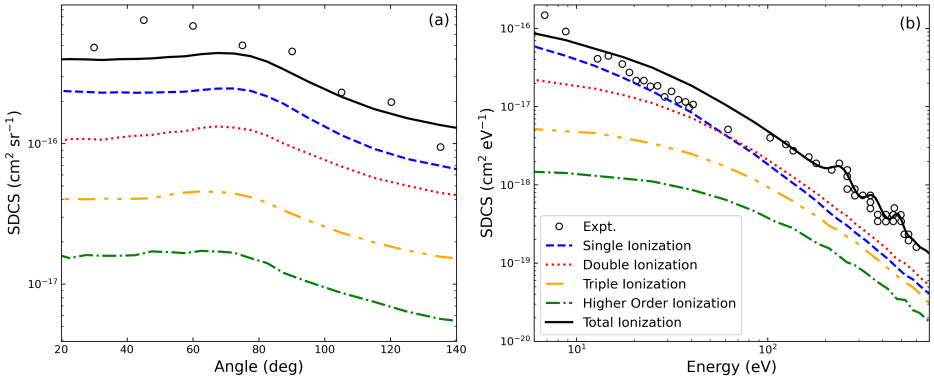

Figure 1. Ad-CTMC singly differential cross-section as a function of the electron emission angle (**a**) and energy (**b**). The experimental data correspond to Agnihotri et al. [21].

3.1. Double Ionization

We now turn our attention to the specific emission geometries under which double electron emission takes place. For a highly charged projectile as C^{6+}, and at the impact energy under consideration, double-electron emission is expected to take place via the two-step-2 (TS2) mechanism, in which the projectile ionizes one electron first and in a subsequent stage the other. Other mechanisms for double electron emission such as the two-step 1 (TS1), in which the projectile first ionizes an electron which then ionizes the second one, and the shake-off (SO), where the fast departure of an emitted electron leads to the rearrangement of the remaining target electrons as a result of the sudden change in the electronic screening of the nuclear charges, are not included in our description.

We note that, as the projectile charge increases, the TS2 mechanism is expected to gain relevance compared to the TS1, while the SO emission is expected to dominate for impact energies much greater than those considered herein. Therefore, the lack of TS1 and SO mechanisms in our calculations was not initially considered relevant for this work. Nevertheless, we pointed out that specific studies should be directed in the future to quantify their specific roles.

In Figure 2, we show a contour plot for the interelectronic angle θ_{12} between the first and second emitted electrons as a function of their respective polar angles θ_1 and θ_2. Structures look very similar and highlight that both electrons are mostly emitted with polar angles (i.e., with respect to the projectile incidence direction) in the range 60°–90° holding an interelectronic angle in the range 60°–120°.

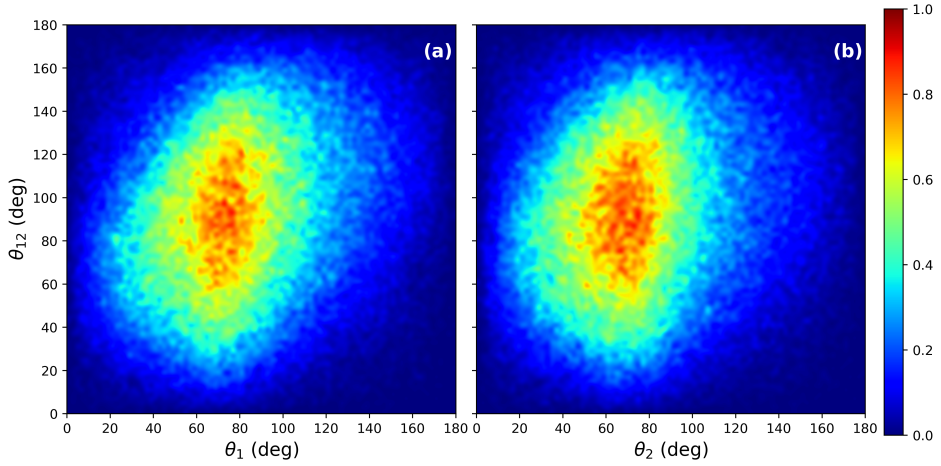

Figure 2. Normalized contour plots for the interelectronic angle θ_{12} between the first and the second emitted electron as a function of their respective polar angles θ_1 (**a**) and θ_2 (**b**) as provided by the Ad-CTMC method.

In Figure 3, we present the contour plots for the energy difference among the emitted electrons $|E_2 - E_1|$ as a function of θ_{12}. We observe that most of the double-ionization events recorded suggest a difference in an energy of less than approximately 20 eV among the emitted electrons. This view is complemented by means of a Dalitz plot shown in Figure 4 in which the ternary variables $\pi_1 = k_1^2/\kappa$, $\pi_2 = k_2^2/\kappa$, and $\pi_3 = k_{12}^2/\kappa$ where k_i is the momentum of emitted electron i, $k_{12} = |\mathbf{k}_1 - \mathbf{k}_2|$, and $\kappa = k_1^2 + k_2^2 + k_{12}^2$, are invoked. Again, we observe that most of the double-ionization events can be associated with lowly energetic electrons emitted at large interelectronic angles. As expected, these results clearly reflect the role played by the postcollisional interaction between the emitted electrons as they leave the reaction region.

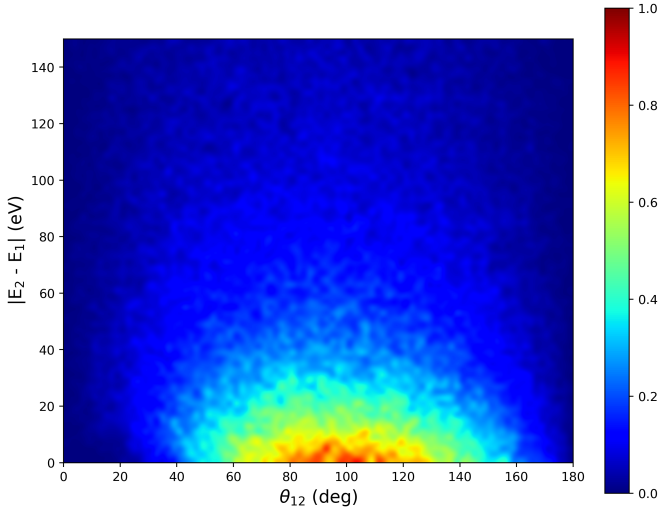

Figure 3. Normalized contour plot of the relative energy of the emitted electrons in double-ionization processes as a function of the interelectronic relative angle.

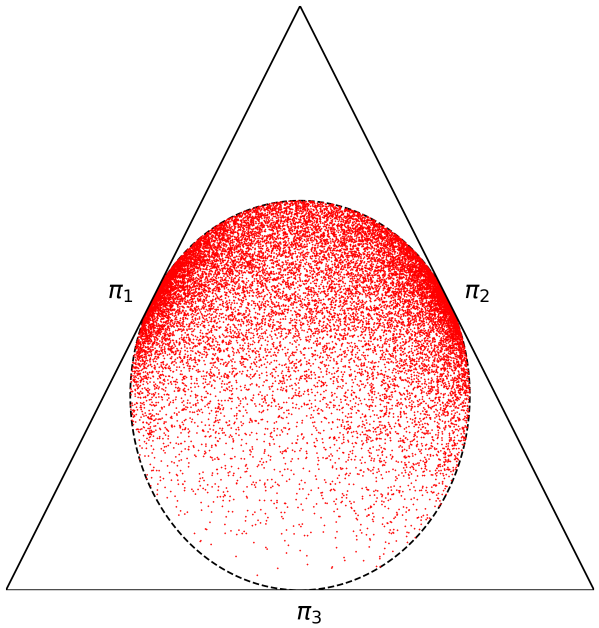

Figure 4. Dalitz plot for double ionization. The ternary variables are described in the text.

We complement the physical picture already acquired for the double-ionization process by examining the reaction region along which the process takes place. In Figure 5, we show a contour plot for the projectile z coordinate value at the moment in which the second electron is emitted (z_2) as a function of the z coordinate value at the moment in which the first electron is emitted (z_1). In both cases, the z coordinate represents the incidence direction of the projectile. We observe that most of the double ionization events take place in the z range (−2 a.u., 2 a.u.) with the projectile transiting a path of less than approximately 1 a.u. between the first and the second ionization.

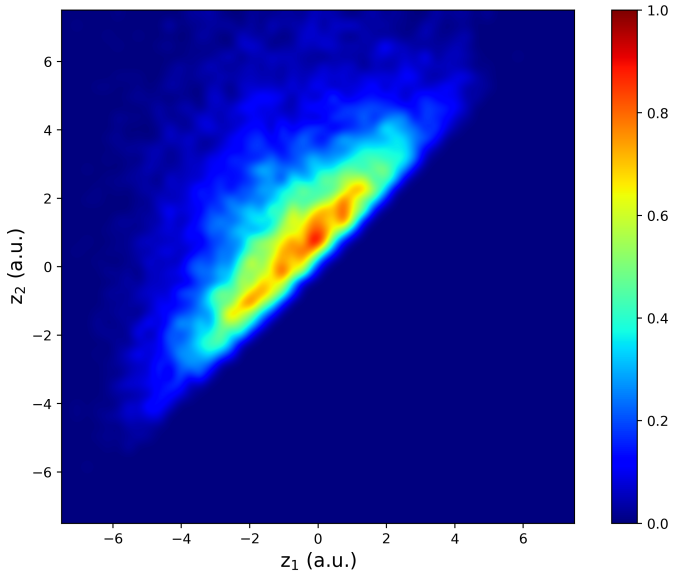

Figure 5. Normalized contour plot for the projectile z coordinate value at the moment in which the second electron is emitted (z_2) as a function of the z coordinate value at the moment in which the first electron is emitted (z_1).

3.2. Triple Ionization

Now, moving to triple ionization, we first want to identify the most favorable angular configurations. In Figure 6, we show the contour plots for θ_{12} vs. θ_1, θ_{13} vs. θ_1 and θ_{23} vs. θ_2 together with a histogram of events for the interelectronic angles θ_{12}, θ_{13} and θ_{23}. From these plots, we deduce that the three electrons are most likely emitted following a three-dimensional arrangement with similar interelectronic angles. These results seem to be in agreement with those previously shown for the double-ionization analysis and indicate that the postcollisional interaction between the emitted electrons hinder the emission of electrons in similar directions.

With the objective of exploring the reaction region for triple ionization, in Figure 7, we show a contour plot for the projectile z coordinate value at the moment in which the third electron is emitted (z_3) as a function of the z coordinate value at the moment in which the first electron is emitted (z_1). In this case, we observe that a large fraction of the triple ionization events occur once the projectile reaches its point of closest approach to the geometrical center of the molecule. A closer inspection (Figure 8) reveals that the peak of the triple ionization events take place in a projectile track path of approximately 2 a.u., however, the whole process can extend with decreasing probability to a path of up to 15 a.u.

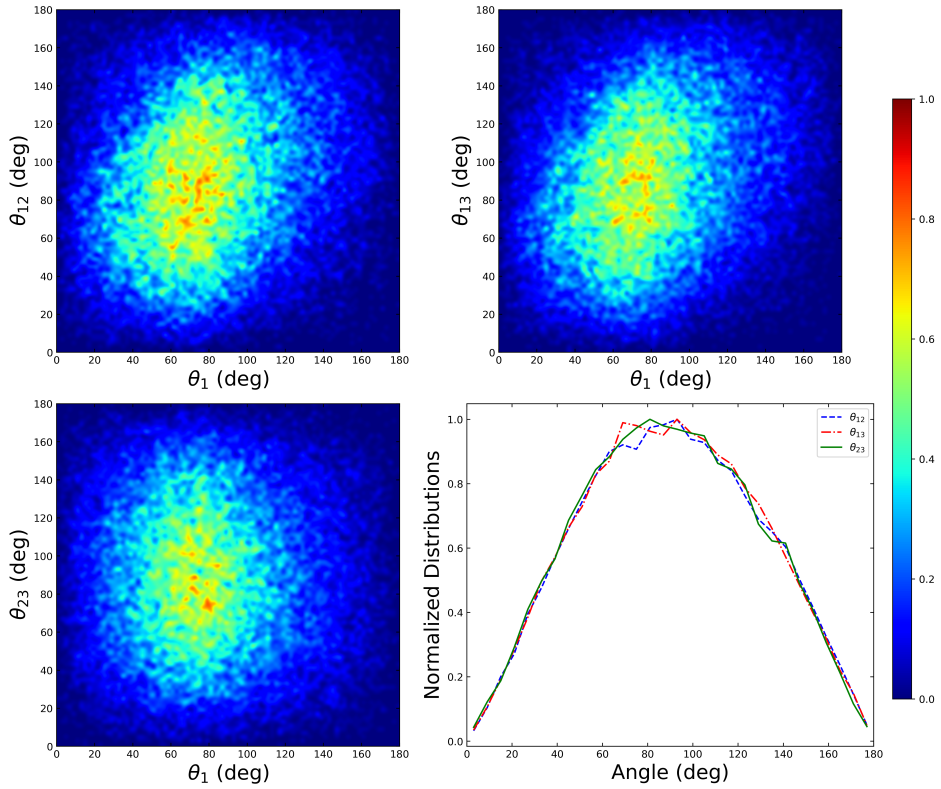

Figure 6. Normalized contour plots θ_{12} vs. θ_1, θ_{13} vs. θ_1 and θ_{23} vs. θ_2 together with a histogram of events for the interelectronic angles θ_{12}, θ_{13} and θ_{23} for triple ionization.

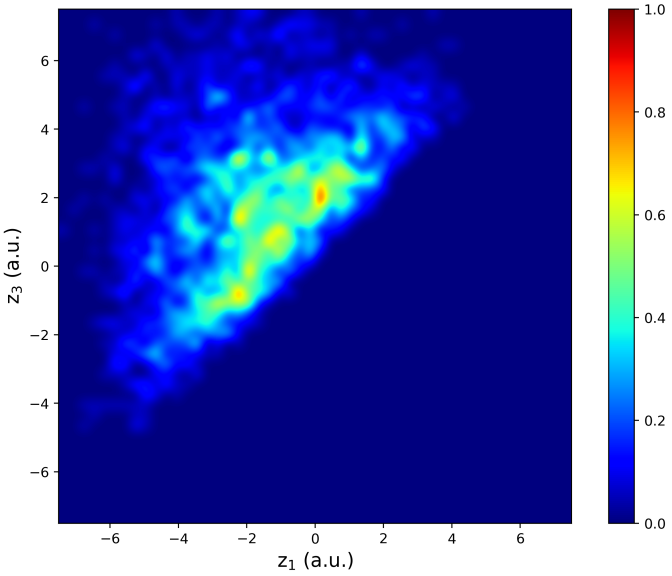

Figure 7. Normalized contour plot for the projectile z coordinate value at the moment in which the third electron is emitted (z_3) as a function of the z coordinate value at the moment in which the first electron is emitted (z_1).

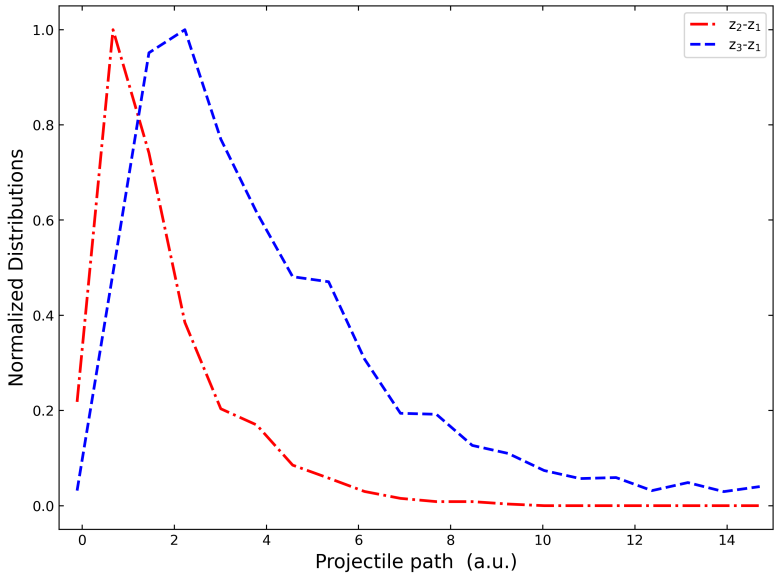

Figure 8. Histogram for the projectile path between the first and second electron removal ($z_2 - z_1$) and the first and third electron removal ($z_3 - z_1$) as predicted by the present Ad-CTMC method.

4. Conclusions

In this work, we recently implemented the Ad-CTMC method introduced to gain further insight into the multiple ionization of uracil by a 3.5 MeV/u C^{6+} impact. In particular, emphasis has been put in determining the emission geometries and reaction region for the double- and triple-ionization processes. Despite the interest in the present problem from a basic science perspective, we recall that accurate differential ionization cross-sections for single and multiple ionization are needed for the Monte Carlo track structure codes designed to simulate irradiation processes on human tissue.

The present results suggest that, for double ionization, both electrons tend to emerge with low energies and at interelectronic angles in the range of 60°–120°. Furthermore, the double ionization process seems to take place in a projectile path window of approximately 2 a.u. In contrast, for triple ionization, the three electrons seem to be most likely emitted following a three-dimensional arrangement with similar interelectronic angles in a projectile path window that extends up to approximately 15 a.u.

Further differential data regarding the ion impact ionization of RNA bases would be desirable at this point. These data would represent an invaluable contribution to help us refine the present theoretical capabilities.

Author Contributions: N.D.C., N.B. and S.O. developed the Ad-CTMC code. N.D.C. and N.B. performed the numerical calculations and contributed to the final manuscript. S.O. contributed to the final manuscript and supervised the project. All authors have read and agreed to the published version of the manuscript.

Funding: This work was supported by Grant No. PGI-24/F084, Secretaría General de Ciencia y Tecnología, Universidad Nacional del Sur.

Data Availability Statement: The data that support the findings of this study are available from the authors upon reasonable request.

Conflicts of Interest: The authors declare no conflict of interest.

References

1. Lisse, C.M.; Dennerl, K.; Englhauser, J.; Harden, M.; Marshall, F.E.; Mumma, M.J.; Petre, R.; Pye, J.P.; Ricketts, M.J.; Schmitt, J.; et al. Discovery of X-ray and Extreme Ultraviolet Emission from Comet C/Hyakutake 1996 B2. *Science* **1996**, *274*, 205–209. [CrossRef]
2. Otranto, S.; Olson, R.E.; Beiersdorfer, P. X-ray emission cross sections following charge exchange by multiply charged ions of astrophysical interest. *Phys. Rev. A* **2006**, *73*, 022723. [CrossRef]
3. Otranto, S.; Olson, R.E.; Beiersdorfer, P. Cometary X-rays: Line emission cross sections for multiply charged solar wind ion charge exchange. *J. Phys. B At. Mol. Opt. Phys.* **2007**, *40*, 1755–1766. [CrossRef]
4. Isler, R.C. An overview of charge-exchange spectroscopy as a plasma diagnostic. *Plasma Phys. Controlled Fusion* **1994**, *36*, 171–208. [CrossRef]
5. Otranto, S.; Olson, R.E. Charge exchange and X-ray emission cross sections for multiply charged ions colliding with H_2O. *Phys. Rev. A* **2008**, *77*, 022709. [CrossRef]
6. Illescas, C.; Errea, L.F.; Méndez, L.; Pons, B.; Rabadán, I.; Riera, A. Classical treatment of ion-H_2O collisions with a three-center model potential. *Phys. Rev. A* **2011**, *83*, 052704. [CrossRef]
7. Liamsuwan, T.; Nikjoo, H. Cross sections for bare and dressed carbon ions in water and neon. *Phys. Med. Biol.* **2013**, *58*, 641–672. [CrossRef]
8. Liamsuwan, T.; Nikjoo, H. A Monte Carlo track structure simulation code for the full-slowing-down carbon projectiles of energies 1 keV u^{-1}-10 MeV u^{-1} in water. *Phys. Med. Biol.* **2013**, *58*, 673–701. [CrossRef]
9. Bhattacharjee, S.; Biswas, S.; Monti, J.M.; Rivarola, R.D.; Tribedi, L.C. Double-differential cross section for ionization of H_2O molecules by 4-MeV/u C^{6+} and Si^{13+} ions. *Phys. Rev. A* **2017**, *96*, 052707. [CrossRef]
10. Bhattacharjee, S.; Bagdia, C.; Chowdhury, M.R.; Monti, J.M.; Rivarola, R.D.; Tribedi, L.C. Energy and angular distribution of electrons ejected from water by the impact of fast O^{8+} ion beams. *Eur. Phys. J. D* **2018**, *72*, 15. [CrossRef]
11. Otranto, S.; Bachi, N.; Olson, R.E. Cross section scaling for H_2O ionization by highly-charged ion impact. *Eur. Phys. J. D* **2019**, *73*, 41. [CrossRef]
12. Bachi, N.; Otranto, S.; Otero, G.S.; Olson, R.E. The role of multiple ionization of H_2O in heavy ion collisions. *Phys. Med. Biol.* **2019**, *64*, 205020. [CrossRef] [PubMed]
13. Bachi, N.; Otero, G.S.; Otranto, S.; Olson, R.E. The role of multiple electron processes for fast ion H_2O collisions. *AIP Conf. Proc.* **2019**, *2160*, 070006.
14. Jorge, A.; Horbatsch, M.; Illescas, C.; Kirchner, T. Classical-trajectory Monte Carlo calculations of differential electron-emission cross sections in fast heavy-ion collisions with water molecules. *Phys. Rev. A* **2019**, *99*, 062701. [CrossRef]
15. Jorge, A.; Horbatsch, M.; Kirchner, T. Multicharged-ion–water-molecule collisions in a classical-trajectory time-dependent mean-field theory. *Phys. Rev. A* **2020**, *102*, 012808. [CrossRef]
16. Lüdde, H.J.; Kalkbrenner, T.; Horbatsch, M.; Kirchner, T. Nonperturbative scaling behavior for net ionization of biologically relevant molecules by multiply charged heavy-ion impact. *Phys. Rev. A* **2020**, *101*, 062709. [CrossRef]
17. Moretto-Capelle, P.; Le Padellec, A. Electron spectroscopy in proton collisions with dry gas-phase uracil base. *Phys. Rev. A* **2006**, *74*, 062705. [CrossRef]
18. Galassi, M.E.; Champion, C.; Weck, P.F.; Rivarola, R.D.; Fojón, O.; Hanssen, J. Quantum-mechanical predictions of DNA and RNA ionization by energetic proton beams. *Phys. Med. Biol.* **2012**, *57*, 2081. [CrossRef]
19. Itoh, A.; Iriki, Y.; Imai, M.; Champion, C.; Rivarola, R.D. Cross sections for ionization of uracil by MeV-energy-proton impact. *Phys. Rev. A* **2013**, *88*, 052711. [CrossRef]
20. Sarkadi, L. Classical treatment of the electron emission from collisions of uracil molecules with fast protons. *Phys. Rev. A* **2015**, *92*, 062704. [CrossRef]
21. Agnihotri, A.N.; Nandi, S.; Kasthurirangan, S.; Kumar, A.; Galassi, M.E.; Rivarola, R.D.; Champion, C.; Tribedi, L.C. Doubly differential distribution of electron emission in ionization of uracil in collisions with 3.5-MeV/u bare C ions. *Phys. Rev. A* **2013**, *87*, 032716. [CrossRef]
22. Agnihotri, A.N.; Kasthurirangan, S.; Nandi, S.; Kumar, A.; Champion, C.; Lekadir, H.; Hanssen, J.; Weck, P.F.; Galassi, M.E.; Rivarola, R.D.; et al. Absolute total ionization cross sections of uracil ($C_4H_4N_2O_2$) in collisions with MeV energy highly charged carbon, oxygen and fluorine ions. *J. Phys. B At. Mol. Opt. Phys.* **2013**, *46*, 185201. [CrossRef]
23. Sarkadi, L. Classical trajectory Monte Carlo model calculations for ionization of the uracil molecule by impact of heavy ions. *J. Phys. B At. Mol. Opt. Phys.* **2016**, *49*, 185203. [CrossRef]
24. Lüdde, H.J.; Horbatsch, M.; Kirchner, T. Proton-impact-induced electron emission from biologically relevant molecules studied with a screened independent atom model. *J. Phys. B At. Mol. Opt. Phys.* **2019**, *52*, 195203. [CrossRef]
25. Abbas, I.; Champion, C.; Zarour, B.; Lasri, B.; Hanssen, J. Single and multiple cross sections for ionizing processes of biological molecules by protons and α-particle impact: A classical Monte Carlo approach. *Phys. Med. Biol.* **208**, *53*, N41. [CrossRef] [PubMed]
26. Olson, R.E.; Ullrich, J.; Schmidt-Bocking, H. Dynamics of multiply charged ion-atom collisions: U^{32+} + Ne. *J. Phys. B Atom. Mol. Phys.* **1987**, *20*, L809. [CrossRef]
27. Cariatore, N.D.; Bachi, N.; Otranto, S. C^{6+}-impact ionization of uracil at MeV/u impact energies: The role of the multiple-ionization channel. *Phys. Rev. A* **2022**, *106*, 012808. [CrossRef]

28. Abrines, R.; Percival, I.C. A generalized correspondence principle and proton-hydrogen collisions. *Proc. Phys. Soc.* **1966**, *88*, 873–883. [CrossRef]
29. Olson, R.E.; Salop, A. Charge-transfer and impact-ionization cross sections for fully and partially stripped positive ions colliding with atomic hydrogen. *Phys. Rev. A* **1977**, *16*, 531–541. [CrossRef]
30. Reinhold, C.O.; Falcón, C.A. Classical ionization and charge-transfer cross sections for H^+ + He and H^+ + Li^+ collisions with consideration of model interactions. *Phys. Rev. A* **1986**, *33*, 3859–3866. [CrossRef]
31. Garvey, R.H.; Jackman, C.H.; Green, A.E.S. Independent-particle-model potentials for atoms and ions with $36<Z\leq54$ and a modified Thomas–Fermi atomic energy formula. *Phys. Rev. A* **1975**, *12*, 1144.
32. Schmidt, M.W.; Baldridge, K.K.; Boatz, J.A.; Elbert, S.T.; Gordon, M.S.; Jensen, J.H.; Koseki, S.; Matsunaga, N.; Nguyen, K.A.; Su, S.; et al. General atomic and molecular electronic structure system. *J. Comput. Chem.* **1993**, *14*, 1347. [CrossRef]